Multi-region and Multi-stage Coordinated Control Method for Resilience Enhancement of Dynamic AC/DC Microgrids

Jiashun Lin, Xiaodong Yuan, Chenyu Zhang, Ruihuang Liu, Shi Chen, and Wei Jiang

***Abstract*—Dynamic microgrids (MGs) possess flexible system topologies and power flow control capabilities, enabling adaptive responses to outages caused by extreme events. This paper proposes a multi-region and multi-stage coordinated control method for the resilience enhancement of dynamic AC/DC MGs, aiming to address limitations arising from rigid electrical boundaries and insufficient coordination of heterogeneous resources during distribution network restoration. The proposed method introduces smart switches (SSWs) to establish dynamic electrical boundaries, thereby partitioning the system into multiple self-operable mini-AC/DC MGs. A novel multi-mode coordinated control scheme is designed to govern grid-forming (GFM) distributed generators (DGs), grid-following (GFL) DGs, and coupling converters (CCs). Specifically, GFM DGs operate in voltage-source mode, maintaining system frequency and voltage via droop control; GFL DGs operate in current-source mode, actively contributing to system regulation through inverse droop control; and CCs manage bidirectional power transfer between AC and DC subgrids based on inverse droop characteristics. Furthermore, a distributed secondary control layer enables the coordinated operation of GFM DGs, GFL DGs, and CCs across multiple regions and stages, ensuring zero-deviation restoration of voltage and frequency, proportional load sharing, and seamless topology reconfiguration. Notably, GFL DGs and CCs remain actively engaged throughout the entire restoration process, thereby maximizing the utilization of available resources and alleviating the capacity burden on GFM DGs. Simulation studies conducted on a 12-bus hybrid AC/DC test system validate the effectiveness of the proposed method in enhancing the resilience and adaptability of hybrid AC/DC MGs under extreme operating conditions.**

***Index Terms*—Microgrid, distributed generator, resilience, coordinated control, secondary control, extreme event, distribution network restoration, smart switch, grid-forming, grid-following.**

Manuscript received: April 25, 2025; revised: July 14, 2025; accepted: September 23, 2025. Date of CrossCheck: September 23, 2025. Date of online publication: November 12, 2025.

This work was supported by National Key Research and Development Program (No. 2023YFB2407400)

J. Lin and W. Jiang (corresponding author) are with the Jiangsu Provincial Key Laboratory of Smart Grid Technology and Equipment, School of Electrical Engineering, Southeast University, Nanjing 210096, China (e-mail: linjiashun@seu.edu.cn; jiangwei@seu.edu.cn).

X. Yuan, C. Zhang, R. Liu, and S. Chen are with the Power Distribution Department, Jiangsu Electrical Power Research Institute, Nanjing 211103, China (e-mail: 1838658@qq.com; zcy530@sina.com; pianoboyliu@163.com; chenshi9004@126.com).

DOI: 10.35833/MPCE.2025.000351

I. Introduction

EXTREME events such as typhoons and earthquakes often result in extensive blackouts, severely compromising the stability and reliability of modern distribution networks [1]-[3]. To mitigate power loss, islanded distribution systems typically initiate restoration by utilizing inverter-based distributed generators (DGs) to form autonomous microgrids (MGs) [4]. MGs, consisting of interconnected loads and distributed energy resources, are capable of operating independently in either grid-connected or islanded mode within predefined electrical boundaries [5]. Numerous studies, like [6] and [7], have highlighted the critical role of MGs in enhancing resilience under extreme conditions. With their ability to safeguard power supply for essential loads and enhance system adaptability, MGs are increasingly recognized as foundational elements of future power grids [8], [9].

Traditional MGs operate within fixed electrical boundaries, and geographically proximate MGs can establish a networked structure through static points of common coupling (PCCs) [10], [11]. While this configuration enhances operational flexibility, it remains constrained by its inherently static nature. To address these limitations, the concept of dynamic MGs has emerged as a more advanced multi-MG structure [12], [13]. Unlike traditional MGs, dynamic MGs feature adjustable electrical boundaries and reconfigurable coupling points, enabling flexible reconfiguration of system topology. By integrating intelligent power electronic devices such as smart switches (SSWs) and soft open points (SOPs), dynamic MGs can adapt to diverse operational scenarios within distribution networks. Recent studies [14], [15] introduce the concept of dynamic electrical boundaries to overcome the limitations of static configurations, enabling the formation of scalable dynamic recovery areas via flexible boundary adjustment using SSWs. Additionally, [16] incorporates boundary adjustment variables into distributed secondary control to facilitate seamless transitions of dynamic electrical boundaries. Further research [17], [18] explores the impacts of communication delays and network topology changes on control strategies for dynamic electrical boundaries.

Compared with a single AC or DC MG, a hybrid AC/DC MG offers enhanced integration capabilities for diverse energy sources, efficiently meets varied load requirements, and provides superior operational flexibility and reliability [19]. Within the dynamic MG framework, the coupling converter

(CC) interconnects the AC and DC subgrids, facilitating optimized power exchange across regions and enhancing overall energy efficiency. Furthermore, the topologies of AC and DC subgrids can be dynamically reconfigured, enabling flexible adjustments of electrical boundaries across regions and energy types. This adaptability offers greater flexibility for system operation in scenarios such as grid optimization, fault recovery, and resilience enhancement. Consequently, dynamic AC/DC MGs are poised to become vital components in the evolution of future distribution networks [20], [21].

However, two significant research limitations exist in the study of dynamic AC/DC MGs. The first one is that conventional restoration strategies overlook the inherent spatial heterogeneity of modern distribution networks. These strategies presume uniform controllability across the entire grid [22], [23], while disregarding two pivotal regional disparities: ① asymmetric renewable energy penetration caused by geographic diversity, and ② historically developed clusters of control modes such as grid-following (GFL) -dominant or grid-forming (GFM)-dominant configurations concentrated in specific regions. Although some recent studies have proposed localized coordination schemes or regionalized control clusters to address such heterogeneity [24], [25], they often operate under static topologies and fail to incorporate dynamic boundary adjustment into the restoration logic. These spatially fragmented characteristics, coupled with rigid inter-regional boundaries, hinder the utilization of complementary resources during cascading failures, thereby forcing systems into suboptimal operational modes, which in turn increase the restoration latency and reduce the overall efficiency.

The second one concerns the insufficient exploration of the role of GFL DG in power sharing and frequency/voltage regulation at the system level. In this study, GFM DG refers to units capable of establishing voltage and frequency references independently, typically realized by inverter-based storage or microturbines. Conversely, GFL DG denotes units that depend on external references for synchronization and regulate their active and reactive power outputs according to system deviations, with photovoltaic inverters and many wind turbine systems serving as representative examples. Existing studies tend to treat GFL DGs as non-controllable resources, overlooking their potential contributions [26]. Several studies have investigated GFM-GFL coordination for synthetic inertia and frequency support [27], [28]. Yet, most of them are confined to steady-state regulation and lack integration into multi-stage restoration processes. As emphasized in IEEE Standard 1547 [29] and supported by research from the Hawaiian Electric Company [30], the participation of GFL DGs in frequency and voltage regulation can significantly enhance the resilience of distribution networks. To address this, the collaborative recovery potential of both GFL and GFM resources should be further explored in the fault recovery processes of distribution networks.

This paper proposes a multi-region and multi-stage coordinated control method for dynamic AC/DC MGs to address the aforementioned limitations. In practice, the restoration of power system is a highly complex process that necessitates coordination among multiple stakeholders. This paper focuses on the role of the multi-region and multi-stage coordinated control method within dynamic AC/DC MGs to enhance the overall system resilience.

1) Multi-region structure

An adaptive multi-region structure is established for dynamic AC/DC MGs, in which SSWs define dynamic electrical boundaries. This enables autonomous segmentation of the system into multiple self-operable mini-MGs based on geographical distribution and control-mode clustering, thereby overcoming rigid boundary constraints in conventional MGs and enhancing resilience under extreme disturbances.

2) Multi-stage operation strategy

A multi-stage operation strategy is developed to guide recovery from local mini-MG bootstrap to regional aggregation and eventually to system-wide resynchronization. The staged process ensures stable voltage/frequency regulation, proportional load sharing, and seamless network transitions at each stage, providing progressive and adaptive resilience enhancement under large-scale disruptions.

3) Multi-mode coordinated control scheme

A novel multi-mode coordinated control scheme is designed to govern heterogeneous resources, including GFM DGs, GFL DGs, and CCs. By combining droop- and inverse-droop-based regulation with distributed secondary control, this scheme achieves accurate voltage/frequency restoration, balanced AC/DC power exchange, and seamless topology reconfiguration. The continuous engagement of GFL DGs and CCs further maximizes resource utilization and alleviates the capacity burden on GFM DGs, thereby improving overall system resilience.

The rest of this paper is organized as follows. Section II introduces the multi-region and multi-stage coordinated control method for dynamic AC/DC MGs. Section III describes the distributed controller design for the multi-mode coordinated control scheme in detail. Section IV details the simulation environment and representative case studies used to demonstrate the effectiveness and resilience of the proposed method. Finally, Section V concludes this paper.

II. Multi-region and Multi-stage Coordinated Control Method

A. Multi-region Structure of Dynamic MGs

In traditional hybrid AC/DC MGs, the system consists of AC subgrids, DC subgrids, and multiple CCs [31]. Power exchange between AC and DC subgrids is managed by CCs, while various DGs with grid-interfacing capabilities directly supply loads. However, such systems are constrained by fixed electrical boundaries, which hamper efficient coordination of power resources across regions. The rigid structure limits the flexibility of power redistribution between subgrids during faults or dynamic load variations [32]. Furthermore, such systems struggle to accommodate the variability of renewable energy generation, potentially resulting in resource underutilization or local load shortages. Additionally, the inefficiency of inter-area coordination under fixed boundaries exacerbates restoration delays and undermines grid resilience and adaptability in extreme scenarios [33].

To address these limitations, the multi-region structure employs SSWs to partition AC/DC subgrids into smaller autonomous units, referred to as mini-AC/DC MGs, as shown in Fig. 1. Each mini-AC/DC MG contains at least one GFM DG to ensure autonomy and may incorporate GFL DGs to enhance flexibility. The multi-region partitioning enables more granular control, allowing rapid responses to faults and load variations while flexibly adjusting electrical boundaries to overcome the rigidity of fixed boundaries. Under the guidance of the system operator, these regions can operate independently or dynamically collaborate with neighboring regions via interconnected SSWs or CCs, thereby facilitating inter-region resource coordination. The system operator can dynamically adjust coordination modes and electrical boundaries based on real-time operating conditions and fault scenarios to optimize resource allocation and recovery efficiency. This multi-region structure enables scalable and region-specific control strategies as well as robust coordination across AC and DC resources, significantly enhancing the overall resilience and adaptability of the system [34].

In this structure, the roles of SSW and CC are explicitly defined.

1) SSWs serve as dynamic boundary regulators, enabling flexible partitioning, fault isolation, and staged reconfiguration of MG topology. They are critical for supporting multi-region organizations and ensuring seamless topology reconfigurations during restoration.

2) CCs act as AC/DC coordinators, ensuring voltage and frequency compatibility, balancing inter-subgrid power flows, and supporting coordination between GFM and GFL DGs.

While this paper focuses on their roles in resilience-oriented restoration, both devices also have the potential to support broader functionalities such as energy optimization, power quality regulation, and hybrid system scheduling under normal operating conditions.

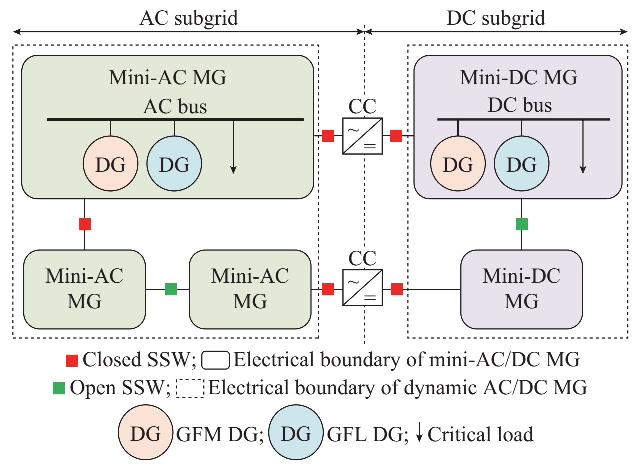

Fig. 1. Multi-region structure of dynamic AC/DC MG.

B. Multi-stage Operation Strategy

Considering that the capability of power system to restore loads following extreme events rapidly is a key indicator of resilience [35], this subsection proposes a multi-stage operation strategy to accelerate load recovery and more comprehensively demonstrate system resilience. Following an extreme event, the multi-region structure of dynamic AC/DC MG operates in three stages, utilizing the coordinated actions of SSWs to manage system topology and power flow flexibly. This adaptability enables the system to accommodate diverse fault scenarios and varying power supply requirements. Figure 2 illustrates the three operational stages, which are described as follows.

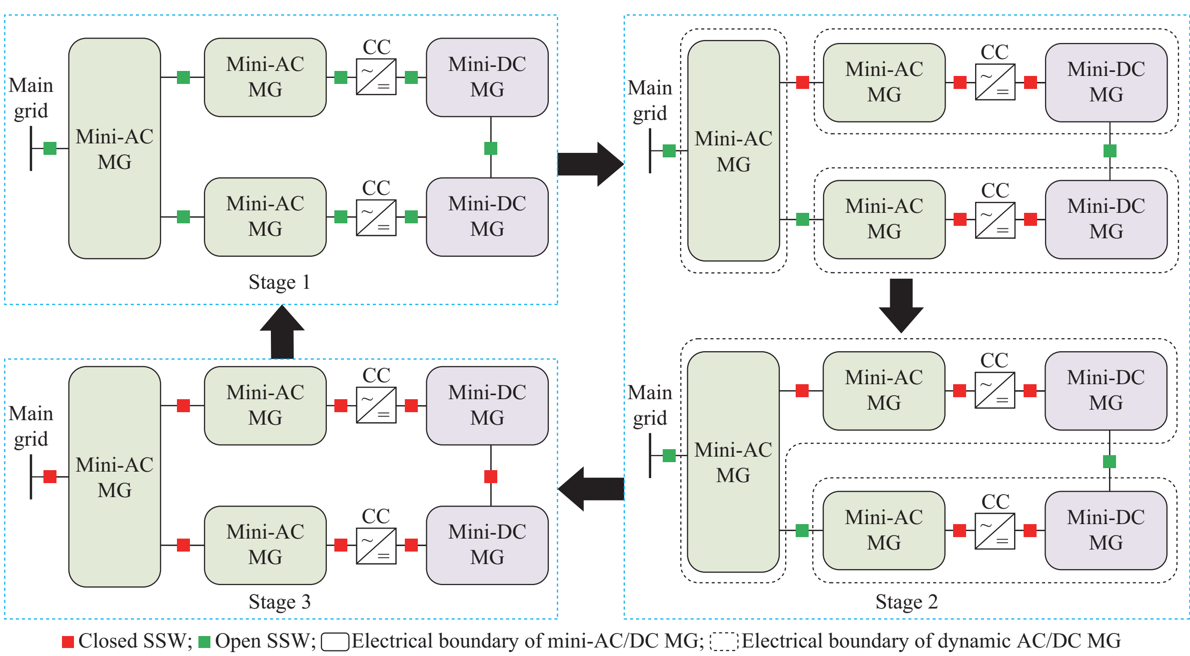

Fig. 2. Multi-stage operation strategy.

1) Stage 1: Voltage and Frequency Establishment Within Mini-AC/DC MGs

In the aftermath of large-scale blackouts, all SSWs are activated, partitioning the system into multiple independent mini-AC/DC MGs. Each mini-AC/DC MG operates autonomously, with its GFM DG initiating a black start process to restore power to critical loads. Concurrently, GFL DGs operate under inverse droop control, supporting GFM DGs in load recovery and alleviating their voltage and frequency regulation burden. The following criteria define the minimum boundaries of a mini-AC/DC MG.

1) Each mini-AC/DC MG must include at least one GFM DG to independently regulate voltage and frequency for stable islanded operation.

2) The total DG capacity within each mini-AC/DC MG must exceed its critical load demand to ensure supply adequacy.

3) Each mini-AC/DC MG is connected to the larger-scale network through a single SSW.

2) Stage 2: Dynamic Adjustment of Electrical Boundaries

The electrical boundaries of resilience-enhanced dynamic AC/DC MGs can be dynamically adjusted through SSW actions. After establishing stable voltage and frequency of mini-AC/DC MGs, the system optimizes the network reconfiguration sequence (i.e., SSW selection) based on current grid faults and operational constraints. These constraints include DG availability, renewable energy generation, load forecasting, and imbalance mitigation. This process determines the optimal system topology—an extensively studied problem that can be addressed using existing techniques [36], [37]. Hence, this paper does not explore this optimization issue in detail. It is worth noting that during the dynamic adjustment of electrical boundaries, SSWs must satisfy specific opening and closing conditions to avoid undesired transients and ensure seamless transitions and stable system operation.

3) Stage 3: Reconnection to Main Grid

After completing dynamic adjustments of electrical boundaries, the system transitions toward pre-event operating state. At this stage, the reconnection to main grid becomes essential. The distribution network then operates as a unified system, with recovery resources coordinating to achieve synchronization with the larger-scale grid. Grid-connected SSWs are closed sequentially once the necessary conditions are met, ensuring smooth transitions and restoring normal operation. To ensure the effectiveness of dynamic adjustments for electrical boundaries and maintain system resilience, only one target SSW is operated at any given time during the topology transition process. Sequential operation of SSWs in a predefined order ensures seamless transitions and leads to the optimal system topology.

To further clarify the system-level recovery strategy, the transition conditions for the three stages are defined as follows.

Stage 1: activated when a wide-area blackout is detected and local GFM DG units with black-start capability are available. Each mini-AC/DC MG is initialized to autonomously restore voltage and frequency.

Stage 2: initiated once mini-AC/DC MGs achieve stable voltage and frequency, and communication links between regions are restored. Electrical boundaries are then adjusted via SSWs if predicted power imbalances or resource gaps can be mitigated through inter-regional coordination.

Stage 3: once the main grid becomes available and synchronization conditions such as frequency, voltage, and phase alignment are satisfied at the PCCs, the recovery areas are reconnected to the larger-scale grid.

These stage transitions are further governed by internal controller variables, which determine the operating modes of DGs.

III. Distributed Controller Design for Multi-mode Coordinated Control Scheme

In this section, a distributed controller design is developed to coordinate DGs and CCs in dynamic AC/DC MGs, thereby enabling multi-region and multi-stage operation. This controller enables effective cooperation between GFM DGs, which establish system stability, and GFL DGs, which follow the references established by GFM DGs. In doing so, the multi-mode coordinated control scheme ensures the overall resilience and stability of dynamic AC/DC MGs.

Dedicated communication networks are designed for the AC subgrids and DC subgrids, denoted as G_{AC} and G_{DC}, respectively. Each network is modeled as a graph $G=(V,E)$, where $V=\{v_1,v_2,\dots,v_n\}$ is the set of DGs and interlinking converters; and E is the set of communication links. The Laplacian matrix of a communication network G is defined as $\boldsymbol{L}=\boldsymbol{D}-\boldsymbol{A}$, where $\boldsymbol{A}=[a_{ij}]$ is the adjacency matrix, with $a_{ij}=1$ if and only if $\{v_i,v_j\}\in E$, and $a_{ij}=0$, otherwise; and $\boldsymbol{D}=\mathrm{diag}(d_{ii})$ is the degree matrix with $d_{ii}=\sum_{j=1}^{n}a_{ij}$.

1) For the AC subgrid, $G_{AC}=(V_{AC},E_{AC})$, where V_{AC} is the set of DGs that communicate with neighbors via links E_{AC}. Its Laplacian matrix is:

$$\boldsymbol{L}_{AC}=\boldsymbol{D}_{AC}-\boldsymbol{A}_{AC} \tag{1}$$

where $\boldsymbol{D}_{AC}$ and $\boldsymbol{A}_{AC}$ are the degree matrix and adjacency matrix of AC subgrid, respectively.

2) For the DC subgrid, $G_{DC}=(V_{DC},E_{DC})$, where V_{DC} is the set of DGs that communicate with neighbors via links E_{DC}. Its Laplacian matrix formulated as:

$$\boldsymbol{L}_{DC}=\boldsymbol{D}_{DC}-\boldsymbol{A}_{DC} \tag{2}$$

where $\boldsymbol{D}_{DC}$ and $\boldsymbol{A}_{DC}$ are the degree matrix and adjacency matrix of DC subgrid, respectively.

In this paper, G_{AC} and G_{DC} are assumed to be connected and they are undirected graphs, ensuring that their Laplacian matrices $\boldsymbol{L}_{AC}$ and $\boldsymbol{L}_{DC}$ are symmetric and balanced. It is important to highlight that this paper emphasizes the distributed secondary control of multiple DGs within the multi-region and multi-stage coordinated control method. Compared with device-level control such as voltage and current loop regulation, the secondary control operates with a significantly slower dynamic response.

A. Coordinated Controller for DGs in AC Subgrid

1) Coordinated Controller of GFM DGs

For GFM DGs, the *P*-*f* and *Q*-*V* droop controls are used to regulate frequency and voltage within the MG, respectively [38]. However, this can cause deviations in system frequency and voltage, degrading overall system performance. Additionally, for dynamic MG configurations, seamless network reconfiguration is critical. When the SSW is opened with non-zero current or closes with asynchronous voltage vectors, undesirable transients can occur, adversely affecting the system performance [16].

To address this, the secondary regulation is incorporated into the droop control for GFM DGs, with two operating modes: coordination within region and reconfiguration between regions. In the coordination mode, the seamless tracking of system frequency and voltage is achieved. In the reconstruction mode, the current through the SSW must be minimized before it is opened and the voltage vector synchronization is ensured before closing, effectively mitigating transients. This control scheme significantly reduces unwanted transients associated with SSW actions. It should be emphasized that GFM DGs ensure zero steady-state deviations only through the combined action of droop control and secondary regulation, while transient deviations are inevitable during power sharing.

The coordinated controller for the i^{th} GFM DG in AC subgrid is formulated as:

$$\begin{cases} \omega_i = \omega_{ref} - m_{i,ac} P_i + \Delta\omega_{i,ac} \\ E_i = E_{ref} - n_{i,ac} Q_i + \Delta E_{i,ac} \end{cases} \tag{3}$$

where ω_i and E_i are the actual operating frequency and voltage amplitude of the i^{th} GFM DG, respectively; ω_{ref} and E_{ref} are the reference operating frequency and voltage amplitude, respectively; $m_{i,ac}$ and $n_{i,ac}$ are the coefficients of designed P-f and Q-V droop control for the i^{th} GFM DG, respectively; P_i and Q_i are the output active and reactive power of the i^{th} GFM DG, respectively; and $\Delta\omega_{i,ac}$ and $\Delta E_{i,ac}$ are the distributed secondary control variables of the i^{th} GFM DG, which are defined as:

$$\Delta\omega_{i,ac} = \underbrace{g_{f,ac}\Delta\omega_i + g_{p,ac}\sum_j a_{ac,ij}\Delta P'_{ij}}_{\Delta\omega_{c,ac}} + \underbrace{g_{\theta,ac}\beta_i\Delta\theta_{SSW,k} + g_{p,ac}\alpha_i\Delta P'_{SSW,k}}_{\Delta\omega_{r,ac}} \tag{4}$$

$$\Delta E_{i,ac} = \underbrace{(1-\beta_i)g_{e,ac}\Delta E_i + g_{q,ac}\sum_j a_{ac,ij}\Delta Q'_{ij}}_{\Delta E_{c,ac}} + \underbrace{g_{e,ac}\beta_i\Delta E_{SSW,k} + g_{q,ac}\alpha_i\Delta Q'_{SSW,k}}_{\Delta E_{r,ac}} \tag{5}$$

where $a_{ac,ij}$ belongs to the AC communication network, indicating whether there is a communication link between the i^{th} and j^{th} GFM DGs ($a_{ac,ij}=1$ if a link exists, and $a_{ac,ij}=0$, otherwise); $g_{f,ac}$, $g_{p,ac}$, $g_{\theta,ac}$, $g_{e,ac}$, and $g_{q,ac}$ are the secondary control gains; $\Delta\omega_i = \omega_i - \omega_{ref}$ and $\Delta E_i = E_i - E_{ref}$ are the deviations of the operating frequency and voltage amplitude from their reference values of the i^{th} GFM DG, respectively; $\Delta P'_{ij} = P'_i - P'_j$ and $\Delta Q'_{ij} = Q'_i - Q'_j$ are the accumulated mismatches of active and reactive power between the i^{th} and j^{th} GFM DGs, respectively; $\Delta E_{SSW,k}$ and $\Delta\theta_{SSW,k}$ are the deviations in voltage amplitude and phase angle between both sides of the SSW before being closed, respectively; $\Delta P'_{SSW,k}$ and $\Delta Q'_{SSW,k}$ are the per-unit active and reactive power of the SSW before being opened, respectively; and α_i and β_i are the switching variables of the i^{th} GFM DG, which are 0-1 binary variables; $\Delta\omega_{c,ac}$ and $\Delta E_{c,ac}$ are the indices for coordination within region; and $\Delta\omega_{r,ac}$ and $\Delta E_{r,ac}$ are the indices for reconfiguration between regions.

When the coordinated controller converges, each term on the right-hand side of (4) and (5) equals zero. The binary switching (0-1) of α_i and β_i results in the formation of diverse operating modes. Table I defines the operating mode of GFM DGs based on the switching variables α_i and β_i, where the corresponding logical combinations and their functional interpretations are summarized. This table clarifies the roles of α_i and β_i across different coordination scenarios.

TABLE I
OPERATING MODE DEFINITIONS OF GFM DGS BASED ON SWITCHING VARIABLES

α_i	β_i	Operating mode	Control objective
0	0	Coordination within region	Maintain voltage/frequency regulation and proportional power sharing
1	0	Reconfiguration between regions (SSW opening)	Minimize power flow through SSW before disconnection
0	1	Reconfiguration between regions (SSW closing)	Ensure seamless SSW closure and re-enable inter-region connection

1) Coordination within region: $\alpha_i=0$ and $\beta_i=0$. In this mode, the system frequency and voltage regulation in the MG is achieved with $\Delta\omega_i=0$ and $\Delta E_i=0$, ensuring zero deviation. The proportional power sharing among DGs within the region is realized by $\Delta P'_{ij}=0$ and $\Delta Q'_{ij}=0$.

2) Reconfiguration between regions (SSW opening): $\alpha_i=1$ and $\beta_i=0$. This mode requires the target SSW to be opened. Building upon the coordination within region, the current through the target SSW is minimized by ensuring $\Delta P'_{SSW,k}=0$ and $\Delta Q'_{SSW,k}=0$, thereby suppressing the transient process caused by opening the closed path. During the opening of the target SSW, the proportional power sharing between physically isolated DGs is suspended.

3) Reconfiguration between regions (SSW closing): $\alpha_i=0$ and $\beta_i=1$. This requires the target SSW to be closed. Building upon the coordination within region, the voltage amplitude and phase angle synchronization on both sides of the target SSW is ensured by setting $\Delta\theta_{SSW,k}=0$ and $\Delta E_{SSW,k}=0$, thereby suppressing transients when SSW is closed.

2) Coordinated Controller of GFL DGs

In the absence of voltage and frequency supports, GFL DGs cannot independently sustain the stable operation and are typically treated as passive units in many restoration strategies. This often leads to underutilization of their available capacity and increases the burden on GFM DGs. To activate their regulation potential, the inverse droop control is applied, allowing GFL DGs to adjust their active and reactive power outputs in response to local voltage and frequency deviations, respectively. This dynamic response mimics the behavior of GFM DGs, enabling GFL DGs to actively contribute to system regulation rather than relying solely on external support [39].

Moreover, by participating in primary control loops, GFL DGs can reduce the real-time regulation burden on GFM DGs, thereby lowering the total required capacity of GFM DGs, especially in regions where the penetration of GFL DG dominates. To further ensure the coordination, a distributed controller aligns the voltage and frequency references across GFL DGs and GFM DGs, stabilizing the local recovery region and enabling seamless progression across multiple recovery stages.

The coordinated controller for the i^{th} GFL DG in AC subgrid is formulated as:

$$\begin{cases} P_i = \lambda_{i,ac}(\omega_{ref} - \omega_i) + \Delta P_{i,ac} \\ Q_i = \eta_{i,ac}(E_{ref} - E) + \Delta Q_{i,ac} \end{cases} \tag{6}$$

where $\lambda_{i,ac}$ and $\eta_{i,ac}$ are the coefficients of designed inverse *P-f* and *Q-V* droop control of the i^{th} GFL DG, respectively; and $\Delta P_{i,ac}$ and $\Delta Q_{i,ac}$ are the active and reactive power deviations under the distributed secondary control of the i^{th} GFL DG, which are defined as:

$$\Delta P_{i,ac} = \underbrace{k_{f,ac}\Delta\omega_i + k_{p,ac}\sum_j a_{ij}\Delta P'_{ij}}_{\Delta P_{c,ac}} + \underbrace{k_{\theta,ac}\beta_i\Delta\theta_{SSW,k} + k_{p,ac}\alpha_i\Delta P'_{SSW,k}}_{\Delta P_{r,ac}} \tag{7}$$

$$\Delta Q_{i,ac} = \underbrace{(1-\beta_i)k_{e,ac}\Delta E_i + k_{q,ac}\sum_j a_{ij}\Delta Q'_{ij}}_{\Delta Q_{c,ac}} + \underbrace{k_{e,ac}\beta_i\Delta E_{SSW,k} + k_{q,ac}\alpha_i\Delta Q'_{SSW,k}}_{\Delta Q_{r,ac}} \tag{8}$$

where $k_{f,ac}$, $k_{p,ac}$, $k_{\theta,ac}$, $k_{e,ac}$, and $k_{q,ac}$ are the secondary control gains; $\Delta P_{c,ac}$ and $\Delta Q_{c,ac}$ are the active and reactive power deviations for coordination within region, respectively; and $\Delta P_{r,ac}$ and $\Delta Q_{r,ac}$ are the active and reactive power deviations for reconfiguration between regions, respectively.

Like the GFM DG in AC subgrid, the binary switching (0-1) of α_i and β_i generates diverse operating modes for the GFL DG in AC subgrid.

B. Coordinated Controller for DGs in DC Subgrid

1) Coordinated Controller of GFM DGs

The GFM DGs employ *P-V* droop control as the primary control and operate in two modes: coordination within region and reconfiguration between regions. In the coordination mode, the secondary regulation of system voltage and power distribution is executed. In the reconfiguration mode, the control is based on the power flow through the target SSW and the voltage amplitude difference between both sides of the target SSW, enabling seamless adjustment of electrical boundaries in the dynamic AC/DC MGs.

The coordinated controller for the i^{th} GFM DG in DC subgrid is formulated as:

$$V_i = V_{ref} - \mu_{i,dc}P_i + \Delta V_{i,dc} \tag{9}$$

where V_i and V_{ref} are the operating and reference voltages of the i^{th} GFM DG, respectively; $\mu_{i,dc}$ is the *P-V* droop gain of the i^{th} GFM DG; and $\Delta V_{i,dc}$ is the voltage deviation under the designed secondary control variable for the i^{th} GFM DG, which is defined as:

$$\Delta V_{i,dc} = \underbrace{(1-\beta_i)g_{V,dc}\Delta V_i + g_{P,dc}\sum_j \tilde{a}_{ij}\Delta P'_{ij}}_{\Delta V_{c,dc}} + \underbrace{g_{V,dc}\beta_i\Delta V_{SSW,k} + g_{P,dc}\alpha_i\Delta P'_{SSW,k}}_{\Delta V_{r,dc}} \tag{10}$$

where $\tilde{a}_{ij}$ belongs to the DC communication network, whose definition is similar to a_{ij}; $\Delta V_i = V_i - V_{ref}$ is the deviation of the operating voltage from its reference value of the i^{th} GFM DG; $\Delta V_{SSW,k}$ is the voltage amplitude deviation between both sides of the target SSW before closing; $g_{V,dc}$ and $g_{P,dc}$ are the secondary control gains; and $\Delta V_{c,dc}$ and $\Delta V_{r,dc}$ are the voltage deviations for coordination within region and reconfiguration between regions, respectively.

When the coordinated controller converges, each term on the right-hand side of (10) equals zero. The binary switching (0-1) of α_i and β_i generates the following diverse operating modes.

1) Coordination within region: $\alpha_i = 0$ and $\beta_i = 0$. In this mode, the system voltage of DC subgrid is regulated with zero deviation through $\Delta V_i = 0$, and the proportional power sharing between DGs within region is achieved by $\Delta P'_{ij} = 0$.

2) Reconfiguration between regions (SSW opening): $\alpha_i = 1$ and $\beta_i = 0$. This mode requires the target SSW to open. Based on the coordination within region, the power flow through the target SSW is minimized by ensuring $\Delta P'_{SSW,k} = 0$, thus suppressing the transient process when the closed path is opened. During the opening of the target SSW, the proportional power sharing between physically isolated DGs is disabled.

3) Reconfiguration between regions (SSW closing): $\alpha_i = 0$ and $\beta_i = 1$. This mode requires the target SSW to be closed. Building on the coordination within region, the voltage amplitude synchronization on both sides of the target SSW is ensured by setting $\Delta V_{SSW,k} = 0$, thus suppressing the transients when SSW is closed.

2) Coordinated Controller of GFL DGs

This paper also designs a coordinated controller for GFL DGs in DC subgrid to fully leverage the system support capabilities. The inverse *P-V* droop control enables GFL DGs to exhibit power droop-like characteristics, and the distributed secondary control is employed to coordinate with GFM DGs in maintaining stable operation within the recovery region.

The coordinated controller for the i^{th} GFL DG in DC subgrid is formulated as:

$$P_i = \lambda_{i,dc}(V_{ref} - V_i) + \Delta P_{i,dc} \tag{11}$$

where $\lambda_{i,dc}$ is the inverse *P-V* droop gain of the i^{th} GFL DG; and $\Delta P_{i,dc}$ is the active power deviation under designed secondary control variable for the i^{th} GFL DG, which is defined as:

$$\Delta P_{i,dc} = \underbrace{(1-\beta_i)k_{V,dc}\Delta V_i + k_{P,dc}\sum_j \tilde{a}_{ij}\Delta P'_{ij}}_{\Delta P_{c,dc}} + \underbrace{k_{V,dc}\beta_i\Delta V_{SSW,k} + k_{P,dc}\alpha_i\Delta P'_{SSW,k}}_{\Delta P_{r,dc}} \tag{12}$$

where $k_{V,dc}$ and $K_{P,dc}$ are the secondary control gains; and $\Delta P_{c,dc}$ and $\Delta P_{r,dc}$ are the active power deviations for coordination within region and reconfiguration between regions, respectively.

Like the GFM DG in DC subgrid, the binary switching (0-1) of α_i and β_i generates diverse operating modes for the GFL DG in DC subgrid.

C. Coordinated Controller for CCs

In dynamic AC/DC MGs, the CCs serve as a bridge connecting the AC and DC subgrids, enabling flexible control of power flow to balance generation and consumption on both AC and DC sides. Reference [22] sets the CC controller identical to the GFM DGs in the DC subgrid to support the operating voltage. However, this design treats the AC subgrid as a non-interactive DG, neglecting the interaction between the CCs and AC subgrid. Considering that both the AC and DC subgrids of dynamic AC/DC MGs are capable of independent grid formation, this paper designs the CC controller to align with the control of GFL DGs in both AC and DC subgrids. The active power output of these CCs is coupled with the frequency of AC subgrid and the voltage of DC subgrid.

The coordinated controller for the i^{th} CC is formulated as:

$$P_i=\varphi_i\eta_{i,cc}(\omega_{ref}-\omega_i)+(1-\varphi_i)\lambda_{i,cc}(V_{ref}-V_i)+\Delta P_{i,cc} \tag{13}$$

$$\Delta P_{i,cc}=\varphi_i\left(k_{f,cc}\Delta\omega_i+k_{P,cc}\sum_j a_{ij}\Delta P'_{ij}+k_{\theta,cc}\beta_i\Delta\theta_{SSW,k}+k_{P,cc}\alpha_i\Delta P'_{SSW,k}\right)+(1-\varphi_i)\left[(1-\beta_i)g_{V,cc}\Delta V_i+g_{P,cc}\sum_j\tilde{a}_{ij}\Delta P'_{ij}+g_{V,cc}\beta_i\Delta V_{SSW,k}+g_{P,cc}\alpha_i\Delta P'_{SSW,k}\right] \tag{14}$$

where $\eta_{i,cc}$ and $\lambda_{i,cc}$ are the coefficients of designed inverse P-f and Q-V droop control of the i^{th} CC, respectively; φ_i is a 0-1 binary variable; $\Delta P_{i,cc}$ is the active and reactive power deviations under the designed secondary control variable for the i^{th} CC; and $k_{f,cc}$, $k_{P,cc}$, $k_{\theta,cc}$, $g_{V,cc}$, and $g_{P,cc}$ are the secondary control gains. The binary switching (0-1) of φ_i generates diverse operating modes for the CC as follows.

1) AC-DC transmission mode: $\varphi_i=1$, which indicates that the AC subgrid connected to the target CC has surplus power, while the DC subgrid has power demand. In this mode, the CC is considered a controllable load from the perspective of the AC subgrid and coordinates with DGs in the DC subgrid to achieve the power sharing and seamless operation of the target SSW.

2) DC-AC transmission mode: $\varphi_i=0$, which indicates that the DC subgrid connected to the target CC has surplus power, while the AC subgrid has power demand. In this mode, the CC is considered a controllable load from the perspective of the DC subgrid and coordinates with DGs in the AC subgrid to achieve the power sharing and seamless operation of the target SSW.

Specifically, the control flag of the CC is dynamically determined by comparing the real-time power surplus or deficit between the AC and DC subgrids. When the AC subgrid has a surplus and the DC subgrid has a deficit, the CC operates in AC-DC transmission mode; conversely, when the DC subgrid has a surplus and the AC subgrid has a deficit, the CC switches to DC-AC transmission mode. The transferable power is determined by a local optimization strategy, which considers available DG capacities, operational constraints, and load forecasts within the interconnected regions, aiming at proportional power sharing. In the simulation studies, a rule-based allocation is adopted for clarity, but the control framework readily supports more advanced optimization algorithms, as demonstrated in [40].

IV. Case Study

The proposed method is evaluated on a 12-bus hybrid AC/DC test system, as depicted in Fig. 3. The test system is partitioned into AC and DC subgrids via a single CC, and further segmented into four mini-AC/DC MGs by two SSWs. It includes four GFM DGs (DG2-DG5) and two GFL DGs (DG1 and DG6), with DG1-DG3 connected to the AC subgrid and DG4-DG6 to the DC subgrid. DG3 and DG4 are interconnected through the CC. The system parameters and control gains are listed in Supplementary Material A Table AI. Specifically, the droop coefficients m_i and n_i are initially derived from the allowable frequency and voltage deviations ($\Delta f_{\max,i}$ and $\Delta V_{\max,i}$) under rated active and reactive power variations (P_i^* and Q_i^*), respectively, i.e., $m_i\approx\Delta f_{\max,i}/P_i^*$ and $n_i\approx\Delta V_{\max,i}/Q_i^*$. In contrast, the inverse droop control coefficients applied to GFL DGs and CCs are not derived analytically in the same manner, as their primary role is to emulate virtual admittance and enable the coordinated power sharing. Their values are initially chosen within reasonable ranges to ensure stability, and then refined through extensive simulation-based tuning to achieve satisfactory dynamic performance and effective restoration behavior. Other control gains such as proportional-integral (PI) parameters for secondary regulation are designed following conventional control principles and further adjusted to guarantee adequate transient response and robustness under different operating conditions.

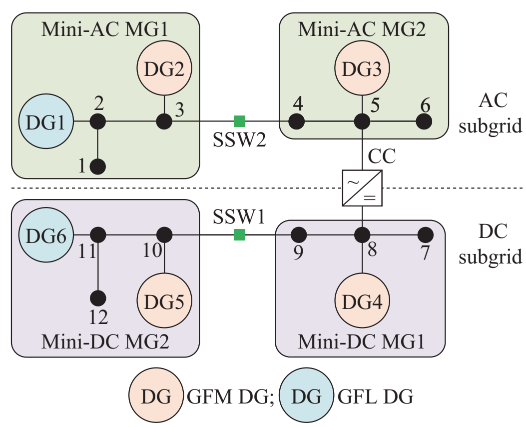

Fig. 3. 12-bus dynamic AC/DC test system.

To emulate the dynamic topology evolution, ideal SSWs are implemented in Simulink. DGs in AC subgrid are interfaced via three-phase full-bridge converters, while DGs in DC subgrid adopt half-bridge converters. The switching sequence of SSWs (t_1-t_8) is predefined to demonstrate a full cycle of regional decoupling and reconnection, ensuring that each SSW experiences both opening and closing operations. This fixed order is intended solely to verify the control design in a comprehensive scenario and does not reflect the optimized switching logic applied in practice. In real deployments, the switching sequence of SSWs would be dynamically determined based on power flow conditions, stability margins, communication availability, and restoration priorities.

For all case studies in this paper, the following assumptions and boundary conditions are adopted.

1) The system starts in the steady state with voltages and frequencies within standard limits.

2) Disturbances (e. g., load changes and faults) are introduced as specified.

3) All DGs are controllable and equipped with the proposed distributed controller, and communication is assumed reliable.

4) Environmental and geographical effects are neglected for conceptual clarity.

5) DG type, control mode (GFM or GFL), and CC settings are defined at the scenario outset.

A. Case I: Voltage and Frequency Establishment of Mini-AC/DC MG

To thoroughly validate the dynamic performance of the proposed distributed controller in coordinating GFM DGs and GFL DGs for system voltage and frequency establishment, a simulation study is conducted using mini-AC MG1 and mini-DC MG2 as case studies. Figure 4 shows the active and reactive power outputs of DG1 and DG2, which participate in the voltage and frequency establishment process, while Fig. 5 shows the voltage and frequency variations in mini-AC MG1.

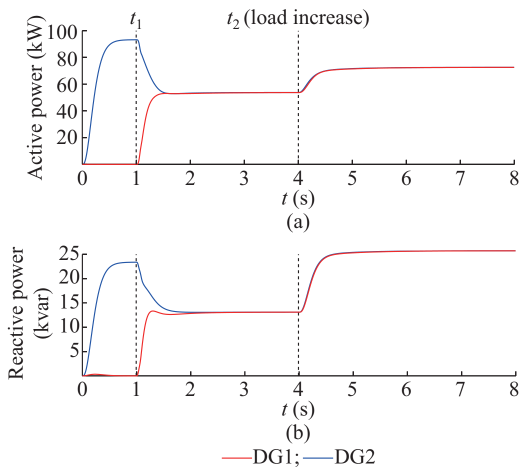

Fig. 4. Active and reactive power outputs of DG1 and DG2. (a) Active power. (b) Reactive power.

From 0 to t_1, DG2 provides initial support for maintaining system voltage and frequency. At t_1, DG2 is activated to participate in voltage and frequency establishment. Once DG2 is engaged, the power is rapidly and proportionally shared between DG1 and DG2, stabilizing both voltage and frequency at rated values.

To further highlight the benefit with both GFM and GFL regulation, we introduce a comparative scenario between hybrid GFM + GFL control and GFM-only control. As shown in Fig. 5(a) and 5(b), the system operating under GFM + GFL control achieves noticeably lower voltage and frequency transients after the load increase at t_2, compared with the GFM-only case. This improvement is attributed to the inverse droop control of GFL DG (DG1), which allows it to dynamically adjust reactive power and assist in stabilizing the AC voltage. Such cooperation significantly reduces the burden on GFM DG (DG2), demonstrating that GFL DG can meaningfully contribute to frequency and voltage regulation when properly coordinated. The power flow patterns also remain stable and consistent during these transitions, as reflected in the corresponding waveforms.

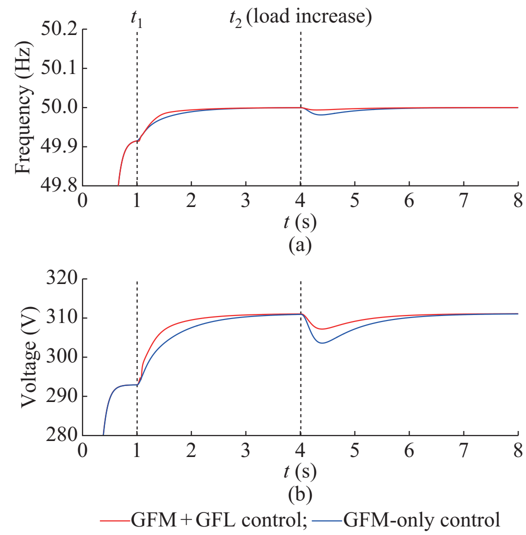

Fig. 5. Voltage and frequency variations in mini-AC MG1. (a) Frequency. (b) Voltage.

Similarly, Fig. 6 illustrates the active power outputs of DG5 and DG6 and the voltage of DG5 during voltage establishment in mini-DC MG1. DG5 and DG6 cooperate to stabilize the system voltage and jointly manage the impact of load increase. The results demonstrate that the proposed distributed controller effectively exploits the contribution of GFL DG in both voltage regulation and power-sharing processes across AC and DC subgrids.

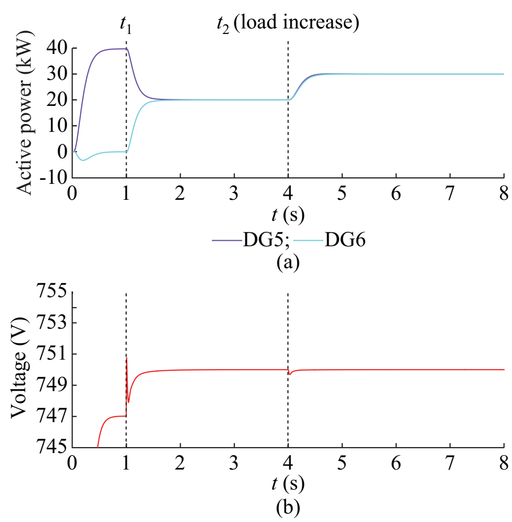

Fig. 6. Active power outputs of DG5 and DG6 and voltage of DG5 during voltage establishment in mini-DC MG1. (a) Active power. (b) Voltage.

B. Case II: Seamless Network Reconfiguration as Requested

To comprehensively evaluate the dynamic performance of the proposed distributed controller in enabling seamless topology reconfiguration of the AC and DC subgrids, the topology of the hybrid AC/DC test system is changed sequentially to create various dynamic MGs, as shown in Fig. 7. The network reconfiguration is requested at time t_1, t_3, t_5, and t_7. Once the operating conditions for seamless topology reconfiguration of the dynamic MG, as described in Section III, are met, the switching operation of SSWs is performed, and the required topology reconfiguration is completed at time t_2, t_4, t_6, and t_8.

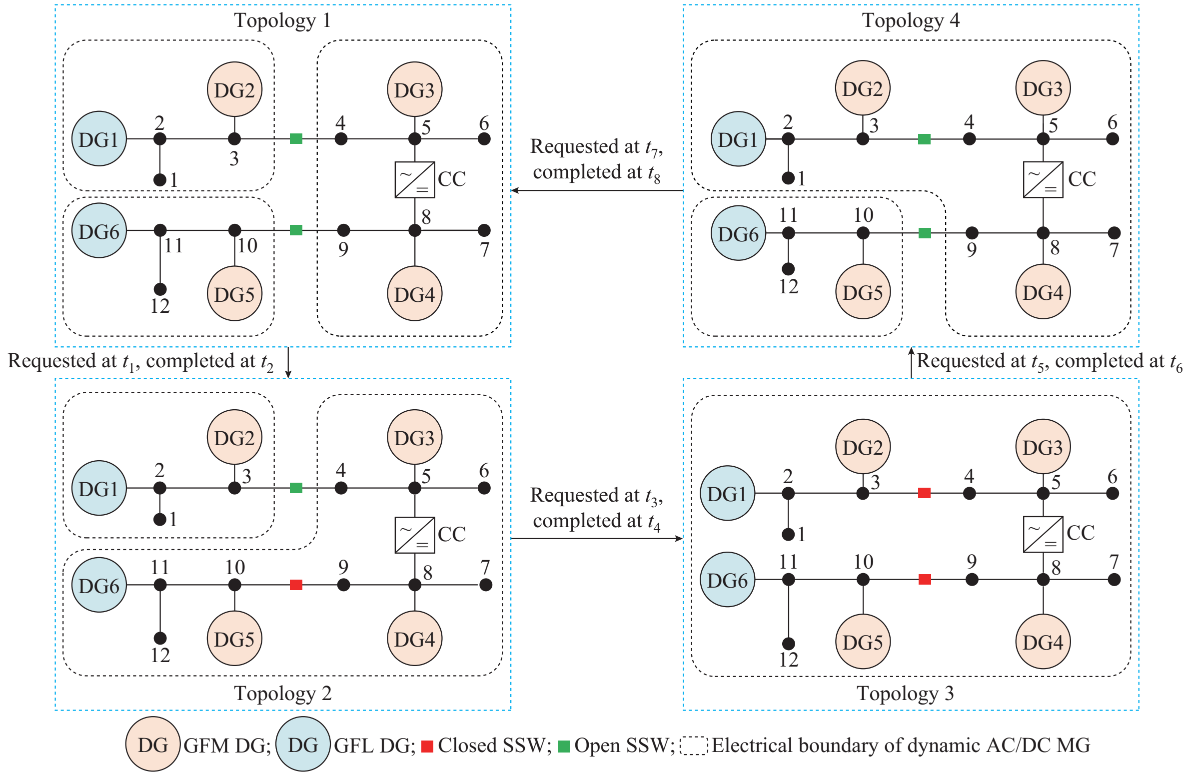

Fig. 7. Sequential topology evolution of hybrid AC/DC test system under multi-stage operation strategy.

Figure 8 presents the frequency and voltage of the AC and DC subgrids, measured at the CC during the topology transitions, where $\Delta f_{\max}$, $\Delta U_{\text{ac,max}}$, and $\Delta U_{\text{dc,max}}$ are the maximum variations of frequency, AC terminal voltage, and DC terminal voltage, respectively. It is observed that, without the seamless topology reconfiguration, when the target SSW undergoes a state change, significant transients and oscillations in the system frequency and voltage are introduced, which severely compromises the stability of the system. However, when the seamless topology reconfiguration is activated, the transients and oscillations induced by the target SSW are significantly mitigated, allowing for a seamless transition. Notably, at the moments when network reconfiguration is requested (i.e., at time t_1, t_3, t_5, and t_7), slight variations in system frequency and voltage are observed. These variations occur as the system executes the control command of seamless topology reconfiguration to ensure that the target SSW meets the conditions required for seamless operation. These experimental results align well with the control theory presented in Section III. The system exhibits enhanced resilience without the occurrence of significant transients or oscillations—a performance level that current advanced technologies have yet to achieve.

Figure 9 illustrates the DG generation during the execution of the multi-stage operation strategy, while Supplementary Material A Fig. A1 presents the operational status of the target SSW during the network reconfiguration process.

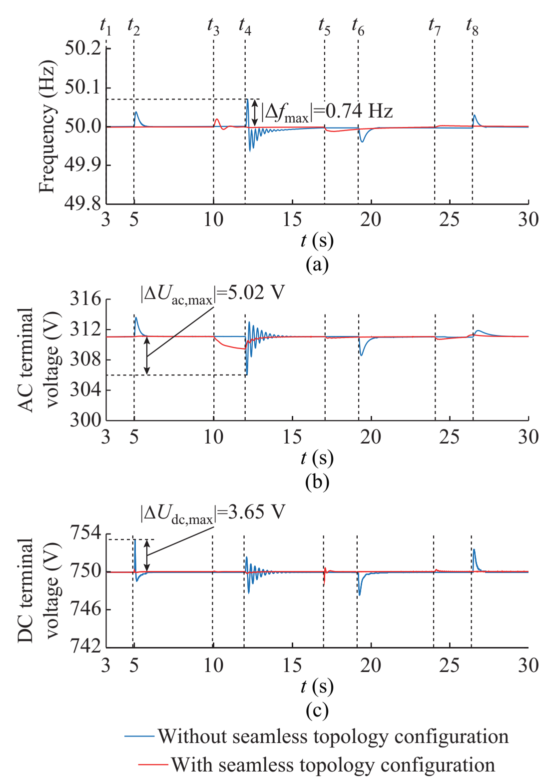

Fig. 8. Frequency and voltage of AC and DC subgrids, measured at CC during topology transitions. (a) Frequency. (b) AC terminal voltage. (c) DC terminal voltage.

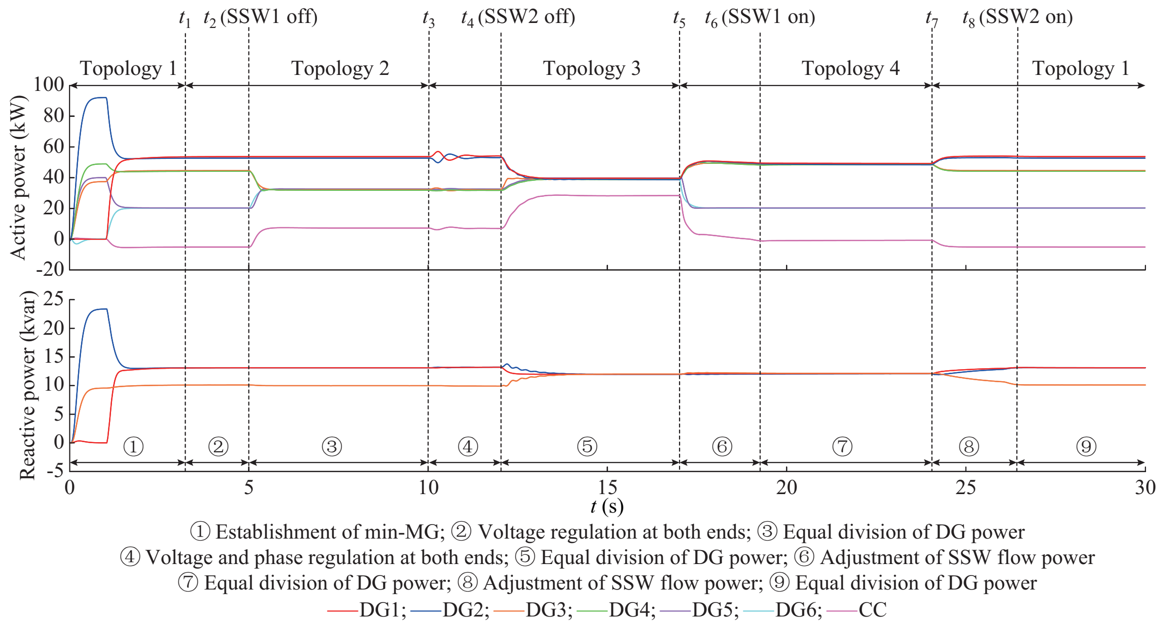

Fig. 9. DG generation during execution of multi-stage operation strategy.

It is evident that, in response to the control command of network reconfiguration, the DGs achieve proportional power sharing. From 0 to t_1, the system operates in topology 1, with all DGs collaboratively establishing voltage and frequency within the region, while the CC operates in AC-DC transmission mode. During this phase, DG4 shares power with DG3 through the CC. From t_1 to t_3, the system operates in topology 2. DG3-DG6 jointly regulate the voltage difference across SSW1 to satisfy the closing condition; SSW1 is closed at t_2, and the system transitions smoothly to topology 2. DG3-DG6 then participate in both active and reactive power sharing. Notably, before the activation of SSW1, the redundant energy of mini-DC MG2 exceeds that of the dynamic MG, which prompts the CC to switch to DC-AC transmission mode after SSW1 is activated. Consequently, DG5 and DG6 share power with DG3 and DG4 via the CC. As shown in Fig. 9, the CC performs a smooth power reversal switching, demonstrating the effectiveness of the proposed distributed controller. From t_3 to t_5, the system operates in topology 3. DG1-DG6 jointly regulate the voltage and phase angle differences across SSW2 to meet the closing condition; SSW2 is closed at t_4, the system transitions smoothly to topology 3, and DG1-DG6 participate in active and reactive power sharing. From t_5 to t_7, the system operates in topology 4. DG1-DG6 jointly regulate the power magnitude through SSW2 to satisfy the opening condition; SSW2 is opened at t_6, the system transitions smoothly to topology 4, and DG1-DG4 are isolated from DG5 and DG6, with each group sharing power internally. The CC again achieves smooth power reversal switching. After t_7, the system is required to switch from topology 4 back to topology 1. DG1-DG4 jointly regulate the power magnitude through SSW1 to satisfy the opening condition; SSW1 is opened at t_8, the system transitions smoothly to topology 1, and each region then operates independently.

C. Case III: Improved System Response with Load Variations

This paper demonstrates that the proposed method enhances the performance of the hybrid AC/DC test system under load variations. A variable power load is connected to bus 3, with its variation shown in Fig. 10. Significant load changes occur at time t_1, t_2, and t_3. Initially, the test system operates under topology 1, where DG3 and DG4 work together to support the load. Rapid power fluctuations can threaten system stability, but the system operator can predict these fluctuations through load forecasting and reconfigure the test system to topology 3, effectively mitigating their impact.

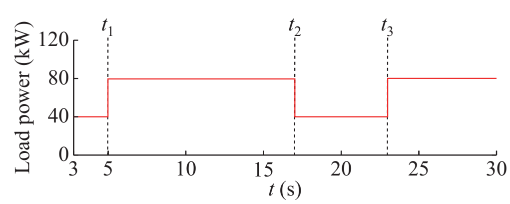

Fig. 10. Load power profile at bus 3.

Figure 11 compares the system performance under topology 1 and topology 3 during load variations. Under topology 1, the load changes at t_1-t_3 cause noticeable oscillations. Notably, although the load variation occurs at bus 9, the power fluctuations on the AC side also induce fluctuations on the DC side due to the power transmission via the CC, which are ultimately suppressed by the multi-mode coordinated control scheme, validating its effectiveness. In contrast, under topology 3, the same load variations are supported by more DGs, and the transients caused by the load changes are significantly reduced, as shown in Fig. 11. This result highlights that the network reconfiguration, enabled by the multi-region structure within the proposed method, improves the performance of hybrid AC/DC test system during load fluctuations.

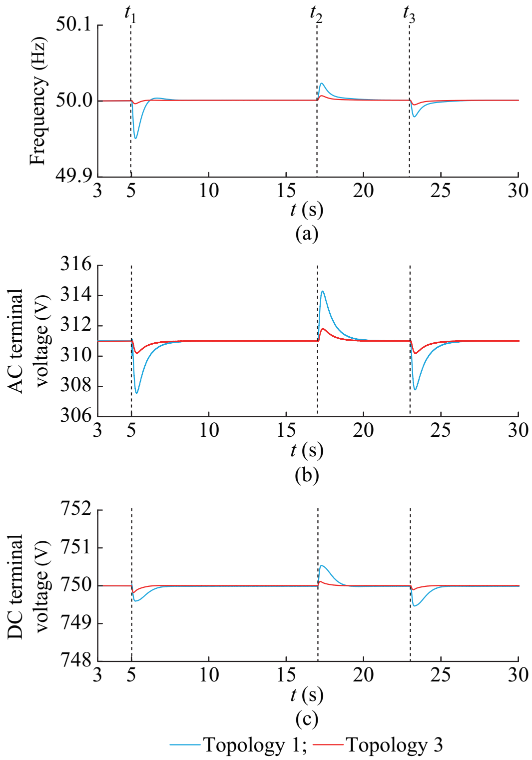

Fig. 11. System performance under topology 1 and topology 3 during load variations. (a) Frequency. (b) AC terminal voltage. (c) DC terminal voltage.

V. Conclusion

In this paper, a multi-region and multi-stage coordinated control method for dynamic AC/DC MGs is developed. The proposed method partitions the feeder into multiple dynamic MG regions and integrates GFM DGs, GFL DGs, and CCs into a multi-stage operation strategy. A multi-mode coordinated control scheme is designed to coordinate the autonomous operation of these heterogeneous components, ensuring that system frequency and voltage are dynamically regulated to rated levels while active and reactive power sharing is proportionally achieved among DGs in both AC and DC subgrids. Moreover, the seamless topology transitions are enabled, supporting adaptive network reconfiguration when required.

The proposed method contributes not only to enhancing system stability and resilience during network reconfiguration but also to broadening the role of GFL DGs in coordinated restoration, thereby improving the overall utilization of distributed energy resources. These features highlight its potential for practical deployment in modern distribution networks with increasing renewable energy penetration.

Future work will extend validation to larger-scale systems with more complex network topologies, diversified DG configurations, and realistic load variations, to provide a more comprehensive assessment of the scalability, adaptability, and robustness of the proposed method in practical operational scenarios. In addition, the systematic benchmarking against representative existing methods will be carried out under unified simulation platforms, alongside thorough parameter sensitivity and robustness analyses. Through these efforts, the generality, engineering applicability, and long-term value of the proposed method will be further demonstrated.

References

[1] L. Yan, M. Sheikholeslami, W. Gong *et al.*, "Architecture, control, and implementation of networked microgrids for future distribution systems," *Journal of Modern Power Systems and Clean Energy*, vol. 10, no. 2, pp. 286-299, Mar. 2022

[2] Y. Ye, H. Wang, P. Chen *et al.*, "Safe deep reinforcement learning for microgrid energy management in distribution networks with leveraged spatial-temporal perception," *IEEE Transactions on Smart Grid*, vol. 14, no. 5, pp. 3759-3775, Feb. 2023.

[3] Y. Nait-Belaid, Y. Fang, Z. Zeng *et al.*, "Communication-aware restoration of smart distribution grids based on optimal allocation of resilience resources," *Journal of Modern Power Systems and Clean Energy*, vol. 13, no. 2, pp. 527-539, Mar. 2025.

[4] J. Huang, G. Lou, W. Gu *et al.*, "Microgrid formation method for load restoration in distribution network with dynamic frequency constraints," *Journal of Modern Power Systems and Clean Energy*, vol. 13, no. 4, pp. 1323-1334, Jul. 2025.

[5] G. C. Kryonidis, E. O. Kontis, A. I. Chrysochos *et al.*, "Power flow of islanded AC microgrids: revisited," *IEEE Transactions on Smart Grid*, vol. 9, no. 4, pp. 3903-3905, Jan. 2018.

[6] G. Jing, B. Huang, R. Wang *et al.*, "Distributed control of networked microgrid with heterogeneous energy storage units considering multiple types of time delays," *Journal of Modern Power Systems and Clean Energy*, vol. 12, no. 6, pp. 1930-1941, Nov. 2024.

[7] X. Yang, H. Liu, W. Wu *et al.*, "Reinforcement learning with enhanced safety for optimal dispatch of distributed energy resources in active distribution networks," *Journal of Modern Power Systems and Clean Energy*, vol. 12, no. 5, pp. 1484-1494, Sept. 2024..

[8] N. Nasser and M. Fazeli, "Buffered-microgrid structure for future power networks; a seamless microgrid control," *IEEE Transactions on Smart Grid*, vol. 12, no. 1, pp. 131-140, Jan. 2021.

[9] S. Li, D. Cao, W. Hu *et al.*, "Multi-energy management of interconnected multi-microgrid system using multi-agent deep reinforcement learning," *Journal of Modern Power Systems and Clean Energy*, vol. 11, no. 5, pp. 1606-1617, Mar. 2023.

[10] J. Lu, C. Qin, Y. Zeng *et al.*, "Collaborative recovery method for cyber-physical distribution system considering multiple coupling constraints," *Journal of Modern Power Systems and Clean Energy*, vol. 13, no. 5, pp. 1752-1762, Sept. 2025.

[11] D. Xu, J. Xu, C. Qian *et al.*, "A pseudo-measurement modelling strategy for active distribution networks considering uncertainty of DGs," *Protection and Control of Modern Power Systems*, vol. 9, no. 5, pp. 1-15, Sept. 2024.

[12] Y. Wang and G. Strbac, "Transient stability-driven planning for the optimal sizing of resilient AC/DC hybrid microgrids," *IEEE Transactions on Power Systems*, vol. 40, no. 3, pp. 2777-2790, May 2025.

[13] Z. Pan, T. Yu, J. Li *et al.*, "Multi-agent learning-based nearly non-iterative stochastic dynamic transactive energy control of networked microgrids," *IEEE Transactions on Smart Grid*, vol. 13, no. 1, pp. 688-701, Jan. 2022.

[14] Y. J. Kim, J. Wang, and X. Lu, "A framework for load service restoration using dynamic change in boundaries of advanced microgrids with synchronous-machine DGs," *IEEE Transactions on Smart Grid*, vol. 9, no. 4, pp. 3676-3690, Dec. 2016.

[15] M. E. Nassar and M. M. A. Salama, "Adaptive self-adequate microgrids using dynamic boundaries," *IEEE Transactions on Smart Grid*, vol. 7, no. 1, pp. 105-113, May 2015.

[16] Y. Du, X. Lu, J. Wang *et al.*, "Distributed secondary control strategy for microgrid operation with dynamic boundaries," *IEEE Transactions on Smart Grid*, vol. 10, no. 5, pp. 5269-5282, Sept. 2019.

[17] Y. Men, L. Ding, J. Zhang *et al.*, "Secondary control fusion in inverter intensive dynamic microgrids for distribution system resiliency enhancement," *iEnergy*, vol. 2, no. 1, pp. 9-13, Mar. 2023.

[18] Y. Du, X. Lu, J. Wang *et al.*, "Dynamic microgrids in resilient distribution systems with reconfigurable cyber-physical networks," *IEEE*

Journal of Emerging and Selected Topics in Power Electronics, vol. 9, no. 5, pp. 5192-5205, Oct. 2021.

[19] S. Paul, A. Sharma, and N. P. Padhy, “Risk constrained energy efficient optimal operation of a converter governed AC/DC hybrid distribution network with distributed energy resources and volt-var controlling devices,” *IEEE Transactions on Industry Applications*, vol. 57, no. 4, pp. 4263-4277, May 2021.

[20] A. Gupta, S. Doolla, and K. Chatterjee, “Hybrid AC-DC microgrid: systematic evaluation of control strategies,” *IEEE Transactions on Smart Grid*, vol. 9, no. 4, pp. 3830-3843, Jul. 2018.

[21] S. K. Sahoo, A. K. Sinha, and N. K. Kishore, “Control techniques in AC, DC, and hybrid AC-DC microgrid: a review,” *IEEE Journal of Emerging and Selected Topics in Power Electronics*, vol. 6, no. 2, pp. 738-759, Jun. 2018.

[22] Y. Deng, W. Jiang, F. Hu *et al*., “Resilience-oriented dynamic distribution network with considering recovery ability of distributed resources,” *IEEE Journal on Emerging and Selected Topics in Circuits and Systems*, vol. 12, no. 1, pp. 149-160, Mar. 2022.

[23] A. Muhtadi, D. Pandit, N. Nguyen *et al*., “Distributed energy resources based microgrid: review of architecture, control, and reliability,” *IEEE Transactions on Industry Applications*, vol. 57, no. 3, pp. 2223-2235, May 2021.

[24] C. Wang, W. Lin, G. Wang *et al*., “Frequency-constrained optimal restoration scheduling in active distribution networks with dynamic boundaries for networked microgrids,” *IEEE Transactions on Power Systems*, vol. 40, no. 3, pp. 2061-2077, May 2025.

[25] K. Pang, C. Wang, N. D. Hatziargyriou *et al*., “Formulation of radiality constraints for optimal microgrid formation,” *IEEE Transactions on Power Systems*, vol. 38, no. 6, pp. 5341-5355, Nov. 2023.

[26] Y. Du, X. Lu, B. Chen *et al*., “Resiliency augmented hybrid AC and DC distribution systems with inverter-dominated dynamic microgrids,” *IEEE Transactions on Smart Grid*, vol. 13, no. 5, pp. 4088-4101, Sept. 2022.

[27] S. Maharjan, C. Bai, H. Wang *et al*., “Distribution system blackstart and restoration using DERs and dynamically formed microgrids,” *IEEE Transactions on Smart Grid*, vol. 16, no. 3, pp. 2100-2114, May 2025.

[28] S. Ke, L. Ding, X. Shi *et al*., “Response characteristics and regulation feasibility of DC charging station controlled by GFM/GFL virtual inertia for grid frequency stability,” *IEEE Transactions on Transportation Electrification*, vol. 11, no. 3, pp. 7743-7758, Jun. 2025.

[29] Z. Zou, J. Tang, X. Wang *et al*., “Modeling and control of a two-bus system with grid-forming and grid-following converters,” *IEEE Journal of Emerging and Selected Topics in Power Electronics*, vol. 10, no. 6, pp. 7133-7149, Dec. 2022.

[30] J. Johnson, J. C. Neely, J. J. Delhotal *et al*., “Photovoltaic frequency-watt curve design for frequency regulation and fast contingency reserves,” *IEEE Journal of Photovoltaics*, vol. 6, no. 6, pp. 1611-1618, Nov. 2016.

[31] S. Peyghami, H. Mokhtari, and F. Blaabjerg, “Autonomous operation of a hybrid AC/DC microgrid with multiple interlinking converters,” *IEEE Transactions on Smart Grid*, vol. 9, no. 6, pp. 6480-6488, Nov. 2018.

[32] Q. Xu, T. Zhao, Y. Xu *et al*., “A distributed and robust energy management system for networked hybrid AC/DC microgrids,” *IEEE Transactions on Smart Grid*, vol. 11, no. 4, pp. 3496-3508, Dec. 2019.

[33] K. P. Schneider, F. K. Tuffner, M. A. Elizondo *et al*., “Evaluating the feasibility to use microgrids as a resiliency resource,” *IEEE Transactions on Smart Grid*, vol. 8, no. 2, pp. 687-696, Mar. 2017.

[34] Z. Li, M. Shahidehpour, F. Aminifar *et al*., “Networked microgrids for enhancing the power system resilience,” *Proceedings of the IEEE*, vol. 105, no. 7, pp. 1289-1310, May 2017.

[35] H. Zhang, C. Chen, S. Lei *et al*., “Resilient distribution system restoration with communication recovery by drone small cells,” *IEEE Transactions on Smart Grid*, vol. 14, no. 2, pp. 1325-1328, Mar. 2023.

[36] A. A. Hamad, M. E. Nassar, E. F. El-Saadany *et al*., “Optimal configuration of isolated hybrid AC/DC microgrids,” *IEEE Transactions on Smart Grid*, vol. 10, no. 3, pp. 2789-2798, Mar. 2018.

[37] H. M. A. Ahmed and M. M. A. Salama, “Energy management of AC-DC hybrid distribution systems considering network reconfiguration,” *IEEE Transactions on Power Systems*, vol. 34, no. 6, pp. 4583-4594, Nov. 2019.

[38] X. Meng, J. Liu, and Z. Liu, “A generalized droop control for grid-supporting inverter based on comparison between traditional droop control and virtual synchronous generator control,” *IEEE Transactions on Power Electronics*, vol. 34, no. 6, pp. 5416-5438, Sept. 2018.

[39] A. Singhal, T. L. Vu, and W. Du, “Consensus control for coordinating grid-forming and grid-following inverters in microgrids,” *IEEE Transactions on Smart Grid*, vol. 13, no. 5, pp. 4123-4133, Mar. 2022.

[40] J. W. Chang, S. Chae, and G. S. Lee, “Distributed optimal power sharing strategy in an islanded hybrid AC/DC microgrid to improve efficiency,” *IEEE Transactions on Power Delivery*, vol. 38, no. 1, pp. 724-737, Feb. 2023.

Jiashun Lin received the M.S. degree in electrical engineering from China University of Mining and Technology, Xuzhou, Jiangsu, China, in 2023. He is currently working toward the Ph.D. degree from the School of Electrical Engineering, Southeast University, Nanjing, China. His research interests include microgrid, secondary control, distributed generation, and cyber-physical system.

Xiaodong Yuan received the M.S. degree in electrical engineering from Southeast University, Nanjing, China, in 2005. He is now a Senior Professor Engineer in Jiangsu Electric Power Research Institute (EPRI), Nanjing, China. He is the Vice Director of the Center of Power System Technology, Jiangsu EPRI. He is also the convener of IEC TC8/WG9 and an expert in TC8/MT2. His research interests include power quality and renewable energy source.

Chengyu Zhang received the Ph.D. degree in electrical engineering from Southeast University, Nanjing, China, in 2016. He is currently a Senior Engineer with Jiangsu Electrical Power Research Institute, Nanjing, China. His research interests include AC/DC distribution and utilization technology and its application.

Ruihuang Liu received the M.S. degree in electrical engineering from North China Electric Power University, Beijing, China, in 2017. He is currently an Engineer with Jiangsu Electrical Power Research Institute,, Nanjing, China. His research interests include AC/DC distribution and utilization technology and its application.

Shi Chen received the Ph.D. degree in electrical engineering from Shanghai Jiao Tong University, Shanghai, China, in 2017. He is currently a Senior Engineer with Jiangsu Electrical Power Research Institute, Nanjing, China. His research interests include power system automation.

Wei Jiang received the B.S., M.S., and Ph.D. degrees in electrical engineering from Southeast University, Nanjing, China, in 2004, 2008, and 2012, respectively. He is currently a Professor of electrical engineering with the School of Electrical Engineering, Southeast University. His research interests include state estimation in distribution network and machine learning-based power system analysis.